Harper, P. W., Sun, L., & Hallett, S. R. (2012). A study on the influence of cohesive zone interface element strength parameters on mixed mode behaviour. *Composites Part A: Applied Science and Manufacturing*, *43*(4), 722-734. https://doi.org/10.1016/j.compositesa.2011.12.016

Published in Composites Part A 2012; 43(4):722–734
DOI: 10.1016/j.compositesa.2011.12.016

A STUDY ON THE INFLUENCE OF COHESIVE ZONE INTERFACE ELEMENT STRENGTH PARAMETERS ON MIXED MODE BEHAVIOR

Paul W. Harper[a], Lu Sun[b] and Stephen R. Hallett[a]

[a] Advanced Composites Centre for Innovation and Science,
University of Bristol, Queen's Building, University Walk, Bristol, BS8 1TR, UK

[b] Aviation Enterprises Ltd, Membury Airfield, Lambourn, Berkshire, RG17 7TJ, UK

Corresponding Author: Stephen.Hallett@bristol.ac.uk

Abstract:

This paper presents a detailed study of the influence of maximum interfacial stress on interface element analyses for composites delamination. The development of the non-linear cohesive zone ahead of a crack tip is analysed with respect to length, stress distribution and mode ratio. The energy absorbed by interface elements is compared with the crack tip strain energy release rate from fracture mechanics analyses. These studies are performed initially on standard fracture toughness specimens, where mode-ratio is fixed by the applied displacement constraints. Results show close agreement with linear elastic fracture mechanics solutions. A simple ply drop specimen is then modelled, where the mode ratio is not constrained by the boundary conditions, and results are compared with the Virtual Crack Closure Technique. In this case maximum interfacial stress has a far greater influence on the numerical results, due to its significant influence on cohesive zone length, mode ratio and energy absorbed.

Keywords: A. Polymer-Matrix Composites, B. Delamination, B. Fracture, C. Finite Element Analysis

Nomenclature

Interface Element Properties:

G_C	Critical Strain Energy Release Rate
K	Interface Element Stiffness prior to damage initiation
σ	Interface Element Stress
σ_{max}	Maximum Interfacial Stress
δ	Interface Element Relative Displacement
δ_e	Interface Element Relative Displacement at damage initiation
δ_f	Interface Element Relative Displacement at final failure

Subscripts *I*, *II* and *m* are used to denote properties under mode I, mode II and mixed mode loading respectively.

Published in Composites Part A 2012; 43(4):722–734
DOI: 10.1016/j.compositesa.2011.12.016

Material Properties:

E_{11}, E_{22}, E_{33}	Young's Moduli
G_{12}, G_{13}, G_{23}	Shear Moduli
ν_{12}, ν_{13}, ν_{23}	Poisson's Ratios

where subscripts 1, 2 and 3 denote the principal material axes.

Geometric Properties:

a	Crack Length
B	Laminate Width
h	Laminate Half Thickness
I	Second Moment of Area

Miscellaneous:

G_T	Total Strain Energy Release Rate (subscripts I and II are used to denote mode I and mode II components)
L_{CZ}	Numerical Cohesive Zone Length
$L_{CZ,f}$	Fully Developed Numerical Cohesive Zone Length in a quasi-static analysis
L_{el}	Element Length
N_{el}	Number of elements within the numerical cohesive zone
P	Load
t	Time
Δ	Cantilever Tip Displacement

1. Introduction

In finite element analysis, cohesive interface elements placed along potential crack propagation paths are becoming widely used for modelling interfacial failure. This is particularly the case for laminated fibre reinforced composite materials, where failure between layers (or plies) is considered to be one of the most detrimental failure modes since it occurs at relatively low loads and results in significant loss of structural properties [1]. Prediction of delamination failure is therefore of great interest to engineers designing composite structures. Interface elements are becoming widely used to predict such delamination failures [2,3,4,5,6,7]. They are also being successfully applied to predicting crack propagation along adhesive bond-lines [8,9,10,11].

Published in Composites Part A 2012; 43(4):722–734
DOI: 10.1016/j.compositesa.2011.12.016

An interface element is a special purpose element that is placed along lines or planes of potential failure in a finite element model. Its behaviour is governed by a traction-displacement curve, in which stress generally increases from zero to the interface material's maximum stress (σ_{max}), before degrading to zero, resulting in complete failure. Figure 1 shows the quasi-static response of a typical interface element formulation, governed by a bi-linear traction-displacement curve, applied to the Double Cantilever Beam (DCB) test for pure mode I fracture behaviour in composite materials [12]. Behaviour under mode II and mixed mode loading is discussed in detail later in this paper. Although the shape of the interface element traction-displacement curve can take numerous forms, one of the conditions for ensuring an accurate delamination analysis is that the total area enclosed must equal the critical fracture energy of the material (G_C).

Figure 1 about here

Although interface elements are constrained to follow a fixed bi-linear traction-displacement response for pure mode I or mode II load cases, there is far less understanding regarding the precise nature of their traction-displacement response under mixed mode loading. This is due to the significant variation in mode-ratio which occurs across the cohesive zone, a region of non-linear deformation that develops ahead of the crack tip. As demonstrated within this paper, the variation in mode ratio is significantly influenced by the maximum mode I and mode II interfacial stress and it is vital that these parameters are carefully chosen in order to conduct accurate delamination analyses.

In order to understand the influence of maximum interfacial stress on crack propagation onset and progression, it is important to consider the development of the cohesive zone as it forms ahead of a stress concentration such as a crack tip. Figure 2 illustrates the development of this zone for pure mode I loading, again using the example of a DCB subject to an increasing tip displacement.

Figure 2 about here

As displacement initially increases, the interface element adjacent to the crack tip rapidly reaches its maximum interfacial stress and moves into the softening region of the traction-displacement response. As tip displacement increases further, element 2 also reaches its maximum stress and begins to experience irreversible deformation, allowing a cohesive zone to be defined. When the cohesive zone initially forms and spans only element 1 and element 2, the stress increase across the cohesive zone is shown as being linear due to the constant stress within each interface element (i.e. due to the discretization of the cohesive zone it is not yet possible to

Published in Composites Part A 2012; 43(4):722–734
DOI: 10.1016/j.compositesa.2011.12.016

determine the precise nature of stress variation across it). As loading continues, more interface elements experience irreversible deformation and the numerical cohesive zone reaches a fully developed length, $L_{CZ,f}$, at the point where the crack tip interface element (element 1) fails completely and the crack begins to propagate. At this point the load also starts to drop on the global load-displacement curve.

It is important to draw a clear distinction between the true physical cohesive zone length, defined as the length over which irreversible damage processes occur ahead of a crack tip and the numerical cohesive zone length, over which interface elements lie on the softening part of their traction-displacement response. For an accurate numerical representation of the physical cohesive zone, the shape of the traction-displacement curve must reflect the stress distribution associated with damage mechanisms occurring ahead of the physical crack tip [13]. However, this stress distribution is very difficult to measure experimentally and for brittle materials such as carbon-epoxy composites, it is often extremely short, typically of the order of 0.3-1mm [14]. If only a global analysis of the structure's load-displacement response is required, results are relatively insensitive to the exact shape of the traction-displacement curve, provided that the correct maximum interfacial stress and fracture toughness are applied [15]. This explains why the bi-linear traction-displacement curve, which is geometrically the most simple form to implement, has become commonly used for delamination analyses [5,6,7]. Furthermore, once a crack has initiated in a structure and a cohesive zone exists, it has been suggested that results are relatively insensitive to the exact value of maximum interfacial stress and only the fracture toughness value is of critical importance [16,17]. In order to conduct an accurate delamination analysis, the mesh must be sufficiently fine to ensure that enough interface elements exist within the cohesive zone length at the point of crack propagation. However, for large structural models, it is also important to avoid the computational expense of an excessively fine mesh. For this reason, the maximum interfacial stress is often set at a value significantly lower than the true physical value because it allows a relatively coarse mesh to be used, whilst still ensuring sufficient interface elements are present within the cohesive zone for an accurate delamination analysis. Previous studies have investigated cohesive zone length and the number of interface elements required within this for an accurate quasi-static crack propagation analysis in simple fracture toughness specimens [16,17]. These found that as long as a minimum of 2-3 interface elements are present within the fully developed cohesive zone, significant reductions in maximum interfacial stress are possible whilst still maintaining results that show close agreement with a fracture mechanics analysis. Such tests have been predominantly carried out on single mode tests only. More recently, Turon et al. [18] have shown that for mixed mode load cases involving standard fracture

toughness specimens, interface elements can undergo a change in mode ratio during failure which is influenced by the ratio of the maximum mode I and mode II interfacial stress values. This change in mode ratio was shown to significantly affect the fracture energy absorbed in each element during failure and recommendations were provided concerning the ratio of maximum interfacial stress values that should be applied to ensure accurate results. The work presented here by contrast focuses on how the maximum interfacial stress affects the length, mode-ratio and stress distribution across the entire cohesive zone and the subsequent influence on global model behaviour. This has been done for both standard fracture toughness specimens, where mode-ratio is fixed by the applied boundary conditions, and in a simple ply drop specimen, where the crack-tip mode-ratio is unconstrained. Since no analytical solutions exist for the ply drop specimen, interface element results are compared with a fracture mechanics based Virtual Crack Closure Technique (VCCT) analysis. In this case, which is more representative of real engineering structural features, the variation in mode-ratio across the cohesive zone ahead of the crack tip is found to be far more heavily influenced by the choice of interfacial strength than the more commonly investigated fracture toughness specimens. Consequently, the energy absorbed across the cohesive zone and the resulting failure load are also more significantly effected, giving far greater importance to the exact choice of interfacial strength values.

An important new finding in the current work, not previously addressed in the literature, is that values of interfacial strength that give reasonable correlation with fracture mechanics analysis results when applied to simple fracture toughness specimens, can give significantly different results when applied in more complex features such as ply drops, more representative of real engineering structures. Although there remains a need for further research in this area, these findings suggest that it is important to restrict the cohesive zone to a relatively short length ahead of the crack tip, requiring values of interfacial strength far closer to their true physical values than is necessary for fracture toughness specimens. This then demands higher mesh densities in order to ensure that a minimum of 2 to 3 elements remain present within the cohesive zone, which has been shown to be necessary in previous investigations for an accurate quasi-static failure analysis [16,17].

The interface element constitutive law and the setup of the numerical models used for this investigation are detailed in sections 2 and 3 respectively. Results showing the influence of interfacial strength on the mode-ratio and stress distribution across the entire cohesive zone, and the consequent effect on global load-displacement behaviour, are then presented in section 4.1 for standard mode I, mode II and mixed-mode fracture toughness specimens. The accuracy of these analyses is evaluated in relation to analytical LEFM solutions. In

Published in Composites Part A 2012; 43(4):722–734
DOI: 10.1016/j.compositesa.2011.12.016

section 4.2, similar results are then presented for a simple ply drop specimen and compared with results from a VCCT analysis. This enables a direct comparison between the sensitivity of the fracture toughness specimen and ply drop specimen results to the choice of interfacial strength values.

2. Interface Element Constitutive Law

The interface elements used for this research take the form of solid hexahedral elements with a small initial thickness, governed by a bi-linear constitutive law. This was developed from a discrete interface element formulation, which has been successfully implemented to model both matrix cracking and delamination within notched composites using the explicit finite element code 'LS-Dyna' [7,19]. The current section provides a brief review of the interface element constitutive law for quasi-static loading, but for full details, the reader should refer to reference [7]. Although it is not rigorously proven in [7] that that the model is thermodynamically consistent, it has been substantially validated against many test cases, both in this and other publications. Spurious energy dissipation however will not give rise to sufficient variation that can explain the effects under investigation in this paper.

The formulation can be illustrated using a single three-dimensional map by representing the normal opening mode (mode I) on the 0 - σ - δ_{normal} plane, and the transverse shear mode (mode II) on the 0 - σ - δ_{shear} plane, as shown in Figure 3. In cases where there is a mode III shear component, the shear displacement, δ_{shear}, becomes the combined resultant of the mode II and mode III shear components. The triangles 0 - $\sigma_{I,max}$ - $\delta_{I,f}$ and 0 - $\sigma_{II,max}$ - $\delta_{II,f}$ are the bi-linear responses in pure opening mode and in pure shear mode respectively. Any point on the 0 - δ_{normal} - δ_{shear} plane represents a mixed-mode relative displacement.

Figure 3 about here

Under load, the interface relationship is initially elastic until reaching the damage onset displacement. For pure mode I or mode II loading, this elastic behaviour is governed by the mode I or mode II elastic stiffness, E_I or E_{II}, until reaching the maximum mode I or mode II interfacial stress. Under mixed mode loading, the damage onset displacement, $\delta_{m,e}$, and maximum interfacial stress, $\sigma_{m,max}$, are calculated using a quadratic damage onset criterion, which has been successfully used to predict mixed mode damage onset in previous investigations [20, 21]:

Published in Composites Part A 2012; 43(4):722–734
DOI: 10.1016/j.compositesa.2011.12.016

$$\sqrt{\left(\frac{max(\sigma_I,0)}{\sigma_{I,max}}\right)^2+\left(\frac{\sigma_{II}}{\sigma_{II,max}}\right)^2}=1 \qquad \text{(Eqn. 1)}$$

When the interface element is further loaded, its strength is assumed to degrade linearly until complete failure. For pure mode I or mode II loading, the corresponding failure displacements, $\delta_{I,f}$ or $\delta_{II,f}$, are calculated using the pure mode I or mode II maximum interfacial stress, $\sigma_{I,max}$ or $\sigma_{II,max}$, combined with the mode I or mode II fracture toughness, G_{IC} or G_{IIC} (see Figure 3). Under mixed mode loading, the failure displacement corresponding to complete decohesion is calculated using the following power law failure criterion, which allows the failure locus shown in Figure 3 to be determined:

$$\left(\frac{G_I}{G_{IC}}\right)^{\alpha}+\left(\frac{G_{II}}{G_{IIC}}\right)^{\alpha}=1 \qquad \text{(Eqn. 2)}$$

where $\alpha \in (1.0 \sim 2.0)$ is an empirical parameter derived from mixed-mode tests, and G_{IC} and G_{IIC} are critical energy release rates for pure mode I (opening) and pure mode II (shear) respectively. When using the power law failure criterion for mixed mode fracture of composite laminates, a best fit to experimental data is generally gained by using a value for α close to 1; Pinho, for example, found a value for α of 1.21 to give a best fit to experimental data for carbon-epoxy prepreg T300/913 [6]. For the mixed mode study presented within this paper, a value of α = 1 has been used. This value was also applied by Jiang et al. [7] for which the numerical analyses gave very close agreement to experimental results when analyzing failure of notched composite specimens.

Under quasi-static loading, a static damage parameter, d_s, is used to track the accumulation of irreversible damage, where:

$$d_s(\delta_m)=\frac{\delta_m-\delta_{m,e}}{\delta_{m,f}-\delta_{m,e}} \qquad \text{(Eqn. 3)}$$

Element failure occurs when d_s reaches a value of unity.

3. Numerical Model Setup

Cohesive zone development, Strain Energy Release Rate (SERR) extraction and crack propagation have initially been investigated under mode I, mode II and mixed mode loading using DCB, 3 point End Notched Flexure (3ENF) and Fixed Ratio Mixed Mode (FRMM) specimens respectively. These studies were then

Published in Composites Part A 2012; 43(4):722–734
DOI: 10.1016/j.compositesa.2011.12.016

extended using an external ply drop specimen, which has no initial pre-crack, but where a sharp stress concentration exists at the edge of each ply drop. It thus remains a fracture driven failure case.

The material properties used for the numerical models are as shown in Table 1. These are based on experimental data for carbon fibre/epoxy HTA/6376C [22], which has been used by a number of other researchers to validate numerical delamination analyses under both static [23] and fatigue loading [24,25]. All of the material properties listed in Table 1 are from reference [22] other than the maximum interfacial stress values and stiffnesses ($\sigma_{I,max}$, $\sigma_{II,max}$, K_I, K_{II}). Interfacial stiffness prior to damage initiation is fixed at a value of 1×10^5N/mm^3, which provides a stiff connection prior to damage initiation without risking the numerical instabilities that can result from the use of higher stiffness values. The maximum mode I interfacial stress is varied between 30MPa and 60MPa and the maximum mode II interfacial stress is varied between 60MPa and 90MPa. This range of values was chosen based on a previous investigation by the authors [16], where it was shown to provide accurate load-displacement analyses for an identical set of fracture toughness specimens. Lowering the maximum interfacial stresses beyond this range was found to result in inaccurate results due to an excessively long cohesive zone. Raising maximum interfacial stress beyond this range also resulted in inaccurate results due to having less than 2-3 elements within the cohesive zone when using identical mesh densities to those applied in the current study. Replicating only the maximum interfacial stresses, which provide accurate load-displacement results under pure mode I and mode II load conditions, allows the current study to focus on whether combinations of these values enable accurate mixed mode analyses to be performed, both for standard fracture toughness specimens and more complex ply drop specimens.

Table 1 about here

Figure 4 and Figure 5 show details of the specimen geometry and numerical model setup for the fracture toughness specimens. Constant stress solid elements were used with one element across the specimen width and symmetry conditions applied along the specimen length. 3 elements were used through the thickness of each cantilever arm. For the DCB and FRMM specimens, a constant element length of 0.125mm was applied along the length of each specimen. This was necessary to ensure that a sufficient number of elements were present within the fully developed cohesive zone to ensure an accurate delamination analysis for all values of maximum interfacial stress applied. For the 3ENF specimen, a constant element length of 0.25mm was applied along the length of the specimen. This longer element length was possible due to the longer cohesive zone lengths under mode II loading. Mass-scaling was applied to maintain a reasonable computational run time of a

Published in Composites Part A 2012; 43(4):722–734
DOI: 10.1016/j.compositesa.2011.12.016

few hours and a global damping factor of 5 was applied to remove high frequency oscillations. Accurate results were maintained by ensuring that the kinetic and damping energy remained negligible compared to the strain energy absorbed by the specimen. Numerical results have been compared with analytical solutions using corrected beam theory (see appendix 1 of reference 16 for equations used).

Figure 4 about here

Figure 5 about here

The external ply drop specimen analysed has a symmetric geometry and consists of 16 UD 0.65mm thick plies; 8 continuous plies in the core and 8 dropped plies (4 on each side of the core). Numerical models of the specimen were constructed to investigate failure. Delamination between the final dropped ply and the core was found to be the most critical failure mechanism, occurring at significantly lower loads than any other potential delamination path between plies. Numerical analyses using interface elements, again performed within LS-Dyna, were compared with analyses conducted using the VCCT within Ansys.

Figure 6 shows the numerical model used for the interface element analyses in LS-Dyna. A quarter model was used with symmetry boundary conditions applied along the base and one lateral surface, and fully fixed boundary conditions applied at the thick end. Constant stress, 8 node solid elements were used for the plies with 5 elements across the specimen width and one element through the thickness of each ply. 0.01mm thick solid interface elements were placed between the core and the final dropped ply, and an element length of 0.2mm was used along the length of each of the ply drop steps. The model was loaded by applying a linearly increasing displacement to all nodes at the thin end. The material properties applied were identical to those used for the fracture toughness specimens, with maximum interfacial stress values again being varied to investigate their influence on the analyses conducted.

Figure 6 about here

A similar model was produced for the VCCT analyses in Ansys but without the interface elements included. 8-node, SOLID185 elements were used with 20 elements across the width and one element through the thickness of each ply. A 0.2mm element length was again used along the length of each dropped ply, having conducted mesh refinement studies to validate that this level of refinement enables converged SERR values to be extracted using the VCCT. The boundary conditions applied were consistent with those specified for the interface element model but in this case, loads were applied to the thin end as an evenly distributed force. To

Published in Composites Part A 2012; 43(4):722–734
DOI: 10.1016/j.compositesa.2011.12.016

perform the VCCT analyses, spring elements were inserted between nodes along the top surface of the core and the bottom surface of the final dropped ply. By changing the stiffness of these spring elements from infinitely large to negligibly small, the crack length was incrementally increased. For each increment of crack growth, the mode I and mode II SERR values were calculated using the spring element forces and their resultant directions. Since a linear static model was used, the SERR values extracted were proportional to the square of the applied load. This meant that the mode ratio extracted for an arbitrary applied load could be used in conjunction with the power law failure criterion (equation 2) to calculate the required load for each increment of crack growth.

6. Results and Discussion

6.1 Fracture Toughness Specimens

To investigate cohesive zone development and SERR extraction under pure mode I loading, a linearly increasing tip displacement was applied to the DCB model using various values of maximum mode I interfacial stress. Figure 7 shows how variation in maximum mode I interfacial stress affects the stress distribution across the cohesive zone at the point of initial crack propagation (i.e. the point at which the initial crack tip element reaches zero stress on its traction-displacement response and fails). For the $\sigma_{I,max}$ = 30MPa case the approximate position on the traction-displacement relationship of selected elements is shown to clarify the process by which the curves have been produced. The same principle applies for all subsequent stress distribution plots presented in this paper and on the charts, solid lines are used for the cohesive zone region and dashed lines for the adjacent elastic region. From Figure 7 it can be seen that the fully developed cohesive zone lengths for maximum interfacial stress values of 30MPa, 45MPa and 60MPa are approximately 1.25mm, 0.9mm and 0.6mm, which gives 10, 7 and 4 entire interface elements within the cohesive zone for the applied element length of 0.125mm.

Figure 7 about here

For the same range of maximum interfacial stress values, Figure 8 shows the global load-displacement results, plotted against the corrected beam theory solution. Despite the significant difference in cohesive zone lengths previously shown in Figure 7, there is no significant difference in the global load-displacement curves, with crack propagation beginning at an almost identical load and displacement. Compared to the analytical solution, a slightly lower stiffness is exhibited in the numerical analyses prior to crack propagation, but there is generally a good level of correlation, with an almost identical match during the crack propagation phase. It should be noted that as shown in the authors' previous work [16], further reductions in interfacial strength lead to

Published in Composites Part A 2012; 43(4):722–734
DOI: 10.1016/j.compositesa.2011.12.016

a significant reduction in stiffness prior to delamination onset due to an excessively long cohesive zone developing ahead of the crack tip. Conversely, depending on the chosen mesh density, increasing interfacial strength can lead to an over-prediction of the crack propagation onset load if there are less than 2 interface elements spanning the fully developed cohesive zone length.

Figure 8 about here

Figure 9 and Figure 10 show the equivalent set of results for the mode II 3ENF. In this case, it is evident from Figure 9 that maximum mode II interfacial stresses of 60MPa, 75MPa and 90MPa result in fully developed cohesive zone lengths of approximately 4.5mm, 3.5mm and 2.5mm, giving 18, 14 and 10 entire interface elements within the cohesive zone for the applied element length of 0.25mm. There is no significant difference between the numerical analyses for this range of maximum interfacial stress values and close agreement is shown with the corrected beam theory solution.

Figure 9 about here

Figure 10 about here

When investigating cohesive zone development under mixed mode loading using the FRMM specimen, a significant variation in mode-ratio was found to occur during the interface element failure process and it is vital that this is understood due to its influence on the total energy absorbed and hence, the nature of crack propagation. To clarify the nature of this failure process, consider the interface element at the crack tip in the FRMM specimen (see Figure 11), initially applying a maximum interfacial stress combination of $\sigma_{I,max}$ = 30MPa and $\sigma_{II,max}$ = 60MPa.

Figure 11 about here

As load is applied, the maximum mixed mode interfacial stress (Equation (1)) is rapidly reached due to the crack tip stress concentration and the element moves onto the softening region of its traction-displacement response. At this stage, there is no cohesive zone behind the element and the mode ratio shows close agreement with that predicted by corrected beam theory. As loading continues, the crack tip element accumulates further damage and elements ahead of it enter the softening region of their traction-displacement response, allowing the cohesive zone to form. The crack tip element experiences a gradual change in mode ratio whilst this occurs, becoming increasingly mode I dominated. When the crack tip element fails and a fully developed cohesive zone has formed, there is a continuous variation in mode ratio along its length. The crack tip element experiences

Published in Composites Part A 2012; 43(4):722–734
DOI: 10.1016/j.compositesa.2011.12.016

predominantly mode I loading, whereas the element at the rear of the zone experiences predominantly mode II loading. The cohesive zone remains at its fully developed length as the crack advances and interface elements now show an identical traction-displacement response, in which they enter the cohesive zone under predominantly mode II loading and fail under predominantly mode I loading.

The traction-displacement response of the initial crack tip element (element 1) is compared against that of the first element to enter the fully developed cohesive zone as the crack begins to advance (element 15) in Figure 12.

Figure 12 about here

These are shown alongside a theoretical traction-displacement response for a fixed mode ratio of G_I/G_{II}=4/3 throughout the interface element failure process (θ=36.9° for this mode-ratio due to G_I and G_{II} being given by $G_I=(\sigma_{I,max}.cos\theta)(\delta_m.cos\theta)$ and $G_{II}=(\sigma_{II,max}.sin\theta)(\delta_m.sin\theta)$ as shown by Figure 1). It is evident that whilst the traction-displacement response of the initial crack tip element (element 1) at first shows close agreement with the fixed mode-ratio response, its mode-ratio becomes increasingly mode I dominated during damage development and it fails at a mode ratio of θ=23.8°. For element 15, the first element to enter the fully developed cohesive zone, the traction-displacement response is initially mode II dominated, but again, there is a gradual increase in mode I loading during damage development. The element finally fails at a very similar mode-ratio to that of element 1 (θ=25.2°).

It can be seen that the mixed mode cohesive zone length, stress distribution and mode ratio variation are influenced by the choice of mode I and mode II maximum interfacial stresses, $\sigma_{I,max}$ and $\sigma_{II,max}$ respectively (Figure 13). In this study, $\sigma_{I,max}$ and $\sigma_{II,max}$ were initially raised together in 15MPa increments, giving $\sigma_{I,max}$: $\sigma_{II,max}$ (MPa) combinations of 30:60, 45:75 and 60:90. This resulted in fully developed cohesive zone lengths of approximately 1.7mm, 1mm and 0.75mm, with 13, 8 and 6 entire interface elements within the cohesive zone for the applied element length of 0.125mm. These lengths are only slightly greater than those gained in the pure mode I analyses and since the pure mode II cohesive zone lengths were significantly longer, this suggests that the mode I stress is having the dominant influence on cohesive zone length. For a mode I maximum interfacial stress of 30MPa, the mode II maximum interfacial stress was also increased from 60MPa to 90MPa (i.e. a 30:90 combination) to give a greater change in the ratio of mode I to mode II strengths. This resulted in only a slight decrease in the fully developed cohesive zone length from approximately 1.7mm to 1.5mm.

Published in Composites Part A 2012; 43(4):722–734
DOI: 10.1016/j.compositesa.2011.12.016

For all of these analyses, there is a significant variation in mode ratio along the length of the cohesive zone (Figure 13b). At the point of initial crack propagation (i.e. element 1 reaching zero stress on its traction-displacement response and failing), the mode ratio is mode I dominated and shows reasonably close agreement for all analyses; approximately 25 degrees for the 30:60 and 30:90 cases, 28 degrees for the 45:75 case and 30 degrees for the 60:90 case. The mode-ratio then exhibits a significant variation along the length of the cohesive zone, becoming increasingly mode II dominated as the interfacial stress increases and the elastic loading region is approached. At the tip of the cohesive zone (i.e. the boundary between the elastic and non-linear loading regions, where an interface element reaches the maximum interfacial stress on its traction-displacement response), the mode ratios for the 30:60, 30:90, 45:75 and 60:90 cases are approximately 80, 75, 73 and 65 degrees respectively. The mode II dominated loading at the tip of the cohesive zone is also reflected by the stress distribution graph (Figure 13a), where the maximum mixed mode interfacial stress is very close to the pure mode II maximum interfacial stress used for each of the cases presented.

Figure 13 about here

The load-displacement curves for this same range of maximum interfacial stress combinations, compared against the corrected beam theory solution, are shown in Figure 14. Although all the analyses show reasonably close agreement with the corrected beam theory solution, there are now more noticeable differences than were exhibited in the pure mode I and pure mode II load-displacement analyses. The load-displacement curves for maximum interfacial stress combinations of 45:75 and 60:90 both show crack propagation to occur at an almost identical upper cantilever tip displacement of 2.7mm and load of 90N. The 30:60 combination results in a slight decrease in the gradient of the load-displacement curve close to the crack propagation load, which results in a slightly greater displacement of 2.8mm at the point of crack propagation, although the crack propagation load remains at 90N. This is likely to be attributable to the longer cohesive zone length for this maximum interfacial stress combination. The gradient of the load-displacement curve for the 30:90 combination closely matches that for the 30:60 combination, but the crack propagation onset load and displacement are increased slightly to 93N and 2.85mm respectively. The influence of maximum interfacial stress variation on the load-displacement response of the FRMM specimen appears broadly consistent with that reported by Turon et al. [18] for a mixed mode bending specimen where $G_I=G_{II}$.

Figure 14 about here

Published in Composites Part A 2012; 43(4):722–734
DOI: 10.1016/j.compositesa.2011.12.016

Although there are some differences in the global load-displacement analyses for each of the maximum interfacial stress combinations, it is evident that they all show reasonable agreement with the analytical corrected beam theory solution. To understand why this level of agreement exists, it is necessary to examine the energy absorbed by interface elements as they undergo failure and the crack progresses. For all cases, the energy absorbed by the initial crack tip element is significantly less than the mixed mode critical fracture energy of 0.373N/mm predicted by Eqn. (2) with α=1 for a fixed mode ratio of G_I/G_{II}=4/3. The initial crack tip element for the 30:60 and 30:90 cases absorbs a critical fracture energy of approximately 0.33N/mm and this increases slightly to approximately 0.34N/mm for the 45:75 and 60:90 cases. After the initial crack tip element has failed and the crack begins to propagate, elements in the cohesive zone absorb increasing amounts of energy before failure, until steady state propagation (Figure 15). This is due to the development of the cohesive zone, which results in them experiencing increasingly mode II dominated loading as they begin to undergo non-linear deformation on the softening part of their traction-displacement response. Once the cohesive zone is fully developed and self-similar crack growth occurs, the traction-displacement response remains fixed as the crack propagates and the total energy absorbed also remains constant at approximately 0.375N/mm for all cases except the 30:90 combination, where the value is approximately 0.4N/mm. The higher fracture energy absorbed by interface elements for the 30:90 combination is consistent with the greater crack propagation load exhibited for this specimen in the load-displacement analyses.

Figure 15 about here

Although results for the FRMM specimen suggest that both the cohesive zone length and the ratio of $\sigma_{I,max}$ to $\sigma_{II,max}$ are having some influence on the results, all of these analyses can still be considered to show reasonable agreement with the analytical solution for this configuration.

6.2. Ply Drop Specimen

In the ply drop specimen the mode ratio is not constrained by the boundary conditions. For the FRMM specimen differences were observed in the mode ratio along the cohesive zone length but these did not significantly affect the global load displacement result. In contrast, in the ply drop specimen it is possible for these differences to influence the overall mode of crack propagation and hence significantly change the final predicted failure load.

Published in Composites Part A 2012; 43(4):722–734
DOI: 10.1016/j.compositesa.2011.12.016

For the ply drop configuration a VCCT analysis was used for comparison of the cohesive zone model results since the mode separation is not influenced by any of the model input parameters. By incrementally advancing a delamination between the final ply drop and the core, critical mode I and mode II SERR values along the delamination front were extracted from the VCCT analysis, using the power law failure criterion (Equation (2)) with alpha = 1. Combining Equation (2) with the assumption that the SERR is proportional to load squared for a linear elastic analysis, an initial failure load of 442MPa can be calculated. As the crack is extended along the ply drop interface, the failure load drops to 418MPa over a length of 0.5mm, which indicates unstable crack growth. The SERR and hence failure load then remain approximately constant until 17mm along the interface, before once again decreasing, indicating unstable crack growth as the delamination approaches the next ply drop in the specimen.

For the same ply drop specimen, interface element analyses were conducted with various maximum interfacial stress combinations. Global load-displacement plots (Figure 16) show a sudden drop at the point where the delamination rapidly propagated back towards the thick section. This is consistent with the VCCT analysis which showed initially unstable crack growth. It is evident that the maximum interfacial stress has a far greater influence on the results than was seen for the FRMM specimen. Combinations of 30:60 and 30:90 result in delamination at an axial stress of approximately 560MPa and 540MPa respectively. By increasing the maximum interfacial stress combinations to 45:75 and 60:90, the delamination stress, conversely, is significantly decreased to 460MPa and 430MPa respectively. These values are in closer agreement to the initial failure stress of 442MPa predicted by the VCCT analysis. The significant differences in failure stress for the interface element analyses can be attributed to the significant changes in energy absorbed during failure and these are now discussed in relation to the cohesive length and variation in mode-ratio across this. From Figure 17(a), it can be seen that when the first element fails, at the tip of the interface between the core and final dropped ply, fully developed cohesive lengths of 3.6mm, 2.0mm, 1.6mm and 0.8mm exist for the 30:60, 30:90, 45:75 and 60:90 maximum interfacial stress combinations respectively. The mode ratio at the crack tip (Figure 17(b)) varies from 30 degrees for the 60:90 case to 45 degrees for the 30:60 case. In all cases this mode ratio increases to approximately pure mode II at the end of the cohesive zone.

Figure 16 about here

Figure 17 about here

Published in Composites Part A 2012; 43(4):722–734
DOI: 10.1016/j.compositesa.2011.12.016

The energy absorbed by interface elements as the crack advances, with respect to both total energy absorbed and the separate mode I and mode II components can be compared to results from the VCCT analysis (Figure 18). In contrast to results for the FRMM specimen, there are now very large differences exhibited between the different maximum interfacial stress combinations. Although the energy absorbed by the initial crack tip element is broadly similar for all cases, ranging from 0.345N/mm for the 60:90 case to 0.4N/mm for the 30:60 case, results then show significant divergence as the crack advances and these explain the large differences in the delamination loads shown by Figure 16.

For both the 30:60 and 30:90 combinations, there is a very large increase in the energy absorbed by interface elements ahead of the initial crack tip element. This can be explained by the longer cohesive zone lengths present in these cases. Since elements at the rear of this zone are experiencing predominantly mode II loading, they initially have higher critical fracture toughness, close to the pure mode II value, and are able to absorb a significant amount of energy before the mode I load component increases and the critical fracture toughness decreases. The development of the long cohesive zone for these maximum interfacial stress combinations also delays the failure of the initial crack tip element and allows a significant increase in load before crack propagation occurs. For the 45:75 and 60:90 combinations, which have shorter cohesive zone lengths, there is much less increase in the energy absorbed by interface elements behind the initial crack tip element. Although loading remains mode II dominated at the end of the cohesive zone for these cases, there is a relatively rapid increase in the mode I component. This means that the energy absorbed during the initial stages of failure when loading is mode II dominated is less significant than for the 30:60 and 30:90 combinations.

Figure 18 about here

Results for the ply drop specimen thus suggest that it is important to restrict the cohesive zone to a very short length ahead of the crack tip, requiring values of interfacial strength far closer to their true physical values than is necessary for fracture toughness specimens. Using a reduced interfacial strength combination of 30:60, the crack propagation load exhibits only a 7% difference from a LEFM analysis for the FRMM specimen (cohesive zone length = 1.7mm), but a 27% difference from the VCCT analysis for the ply drop specimen (cohesive zone length = 3.6mm), even though this remains a fracture driven failure case due to the stress concentration at the ply termination. When the interfacial strength combination is raised to 60:90, closer to realistic physical values, the cohesive zone length is reduced to 0.8mm for the ply drop specimen and the crack propagation load is within 3% of the VCCT analysis. This also means that higher mesh densities may be required when modelling structural

features such as ply drops, in order to ensure that a minimum of 2-3 elements remain present within the cohesive zone, which has been shown to be necessary in previous investigations for an accurate quasi-static failure analysis [16,17].

6. Conclusions

This paper has examined the application of cohesive interface elements to delamination in composite materials. In particular it has paid close attention to the mixed mode loading case and the influence of input parameters, not only on overall results but also the mechanisms by which variable results occur. In simple fracture toughness specimens where a significant pre-crack exists and the crack tip mode ratio is fixed by the applied boundary conditions, accurate delamination analyses can be achieved using a relatively wide range of maximum interfacial stress values in the interface element constitutive law. When modelling more complex structural geometries, where the crack tip mode ratio is not fixed by the boundary conditions, results show far greater sensitivity to maximum interfacial stress. In such cases, a much narrower range of values, approaching those of the material's true strengths, are valid to gain good agreement with a fracture mechanics analysis. The results obtained in this paper for a simple ply drop specimen suggest that the accuracy of the analysis is highly dependent on the length of the cohesive zone. The long cohesive zone lengths which result from the use of low maximum interfacial stress values tend to result in a significant over-prediction of the crack propagation load due to the variation in mode-ratio across the cohesive zone. The interface elements absorb a large amount of energy when they initially enter the cohesive zone due to the mode II dominated loading in this region and the high value of mode II fracture toughness relative to its mode I counterpart. This results in the total fracture energy absorbed at the point of failure being far greater than the value predicted by a linear elastic fracture mechanics analysis, where only the mode-ratio at the crack tip itself affects the results. Close agreement with a fracture mechanics analysis can only be gained when the cohesive zone length is relatively short, obtained by using realistic values for interfacial stress. This may require higher mesh densities in order to ensure that a minimum of 2-3 elements remain present within the cohesive zone.

References

[1] Harris,B (Ed.) (2003) Fatigue in Composites. Woodhead Publishing Ltd, Cambridge. 742 p. (Chapter 6: Delamination Fatigue (Martin,R), p173-188)

[2] Petrossian,Z; Wisnom,MR. Prediction of delamination initiation and growth from discontinuous plies using interface elements. Composites Part A: Applied Science and Manufacturing 1998;29A:503-515.

[3] Chen,J; Crisfield,M; Kinloch,AJ; Busso,EP; Matthews,FL; Qiu,Y. Predicting Progressive Delamination of Composite Material Specimens via Interface Elements. Mechanics of Composite Materials and Structures 1999;6:301-317.

[4] Crisfield,MA; Alfano,G. Finite element interface models for the delamination analysis of laminated composites: mechanical and computational issues. International journal for numerical methods in engineering 2000;50:1701-1736.

[5] Camanho,PP; Davila,CG; De Moura,MF. Numerical Simulation of Mixed-mode Progressive Delamination in Composite Materials. Journal of Composite Materials 2003;37:1415-1424.

[6] Pinho,ST; Ianucci,L; Robinson,P. Formulation and implementation of decohesion elements in an explicit finite element code. Composites Part A: Applied Science and Manufacturing 2006;37:778-789.

[7] Jiang,WG; Hallett,SR; Green,BG; Wisnom,MR. A concise interface constitutive law for analysis of delamination and splitting in composite materials and its application to scaled notched tensile specimens. International journal for numerical methods in engineering 2007;69:1982-1995

[8] Camanho,PP; Davila,CG; Pinho,ST. Fracture Analysis of Composite Co-cured Structural Joints Using Decohesion Elements. Fatigue Fract Engng Mater Struct, 2003;27:745-757.

[9] Blackman,BRK; Hadavinia,H; Kinloch,AJ; Williams,JG. The use of a cohesive zone model to study the fracture of fibre composites and adhesively-bonded joints. International Journal of Fracture 2003;119:25-46.

[10] Li,S; Thouless,MD; Waas,AM; Schroeder,JA; Zavattieri,PD. Mixed-mode cohesive-zone models for fracture of an adhesively bonded polymer-matrix composite. Engineering Fracture Mechanics 2006;73:64-78.

[11] Goyal,VK; Johnson,ER. Predictive strength-fracture model for composite bonded joints. Composite Structures 2008;82:434-446.

[12] ASTM D5528-01(2007)e1 Standard Test Method for Mode I Interlaminar Fracture Toughness of Unidirectional Fiber-Reinforced Polymer Matrix Composites.

[13] Shet,C; Chandra,N. Effect of the Shape of traction-displacement cohesive zone curves on the fracture response. Mechanics of Advanced Materials and Structures 2004;11:249-275.

[14] Cox,B; Yang,Q. In Quest of Virtual Tests for Structural Composites. Science 314, 1102 (2006)

[15] Cox,B; Yang,Q. Cohesive Models for damage evolution in laminated composites. International Journal of Fracture 2005;133:107-137.

[16] Harper,P; Hallett,SR. Cohesive zone length in numerical simulations of composite delamination, Engineering Fracture Mechanics 2008;75:4774-4792.

[17] Turon,A; Davila,CG; Camanho,PP; Costa,J. An engineering solution for mesh size effects in the simulation of delamination using cohesive zone models. Engineering Fracture Mechanics 2007;74:1665-1682.

[18] Turon, A.; Camanho, P.P.; Costa, J.; Renart, J. Accurate simulation of delamination growth under mixed-mode loading using cohesive elements: Definition of interlaminar strengths and elastic stiffness. Composite Structures 2010;92:1857-1864.

[19] Li,X; Hallett,SR; Wisnom,MR. Predicting the effect of through-thickness compressive stress on delamination using interface elements, Composites Part A: Applied Science and Manufacturing 2008;39: 218-230.

[20] Brewer JC, Lagace PA. Quadratic stress criterion for initiation of delamination. Journal of Composite Materials 1988; 22:1141-1155.

[21] Cui W, Wisnom MR, Jones M. A comparison of failure criteria to predict delamination of unidirec tional Glass/Epoxy specimens waisted through the thickness. Composites 1992; 23: 158-166.

[22] Asp,LE; Sjogren,A; Greenhalgh,ES. Delamination Growth and Thresholds in a Carbon/Epoxy Composite Under Fatigue Loading. Journal of Composites Technology and Research 2001;23:55-68.

[23] Borg,R; Nilsson,L; Simonsson,K. Simulating DCB, ENF and MMB experiments using shell elements and a cohesive zone model. Composites Science and Technology 2004;64:269-278.

[24] Robinson,P; Galvanetto,U; Tumino,D; Belluci,G. Numerical simulation of fatigue-driven delamination using interface elements. International Journal for Numerical Methods in Engineering 2004;63:1824-1848.

[25] Turon,A; Costa,J; Camanho,PP; Davila,CG. Simulation of delamination in composites under high-cycle fatigue.Composites Part A: Applied Science and Manufacturing 2007;38:2270-2282.

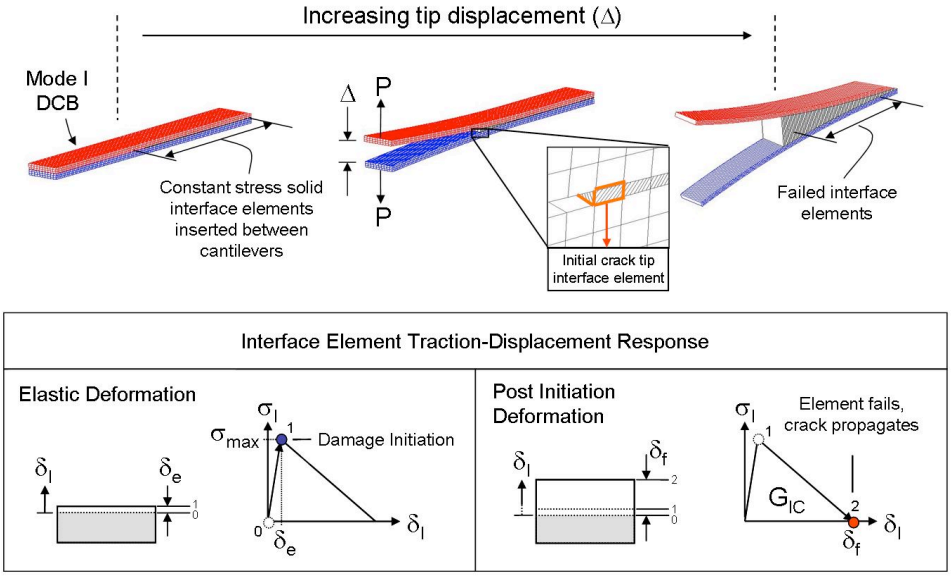

Figure 1: The bi-linear traction-displacement curve

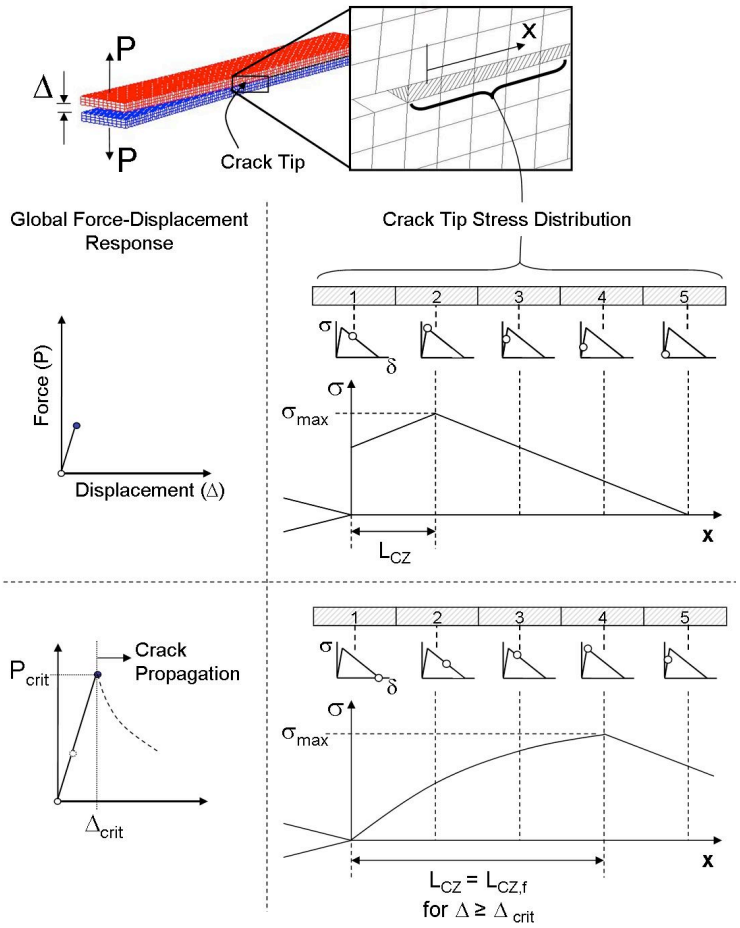

Figure 2: Cohesive Zone Development in a mode I DCB

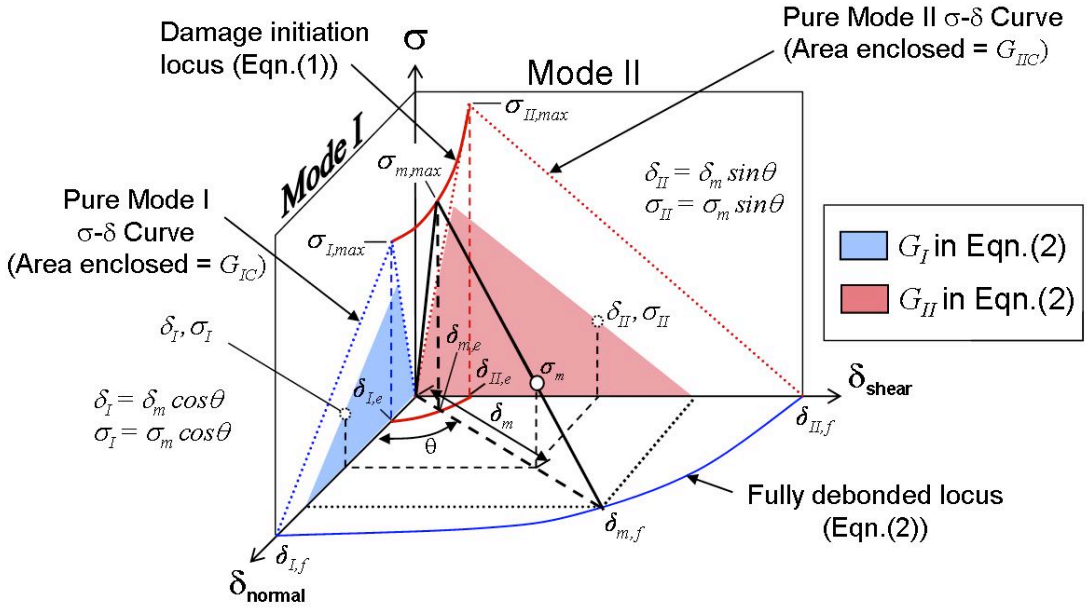

Figure 3: The bi-linear traction-displacement response

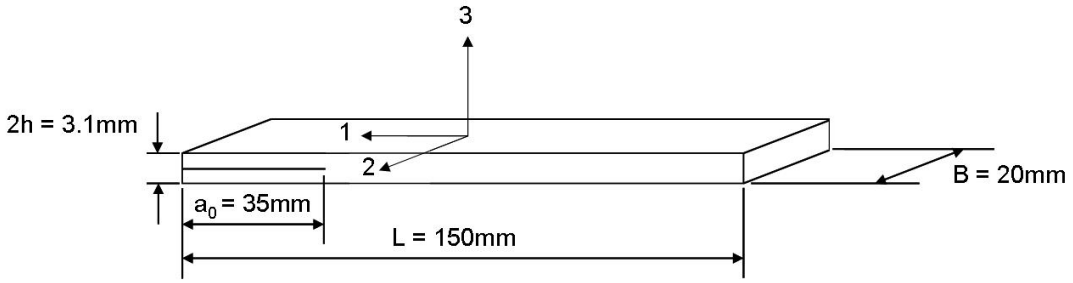

Figure 4: Fracture Toughness Specimen Geometry

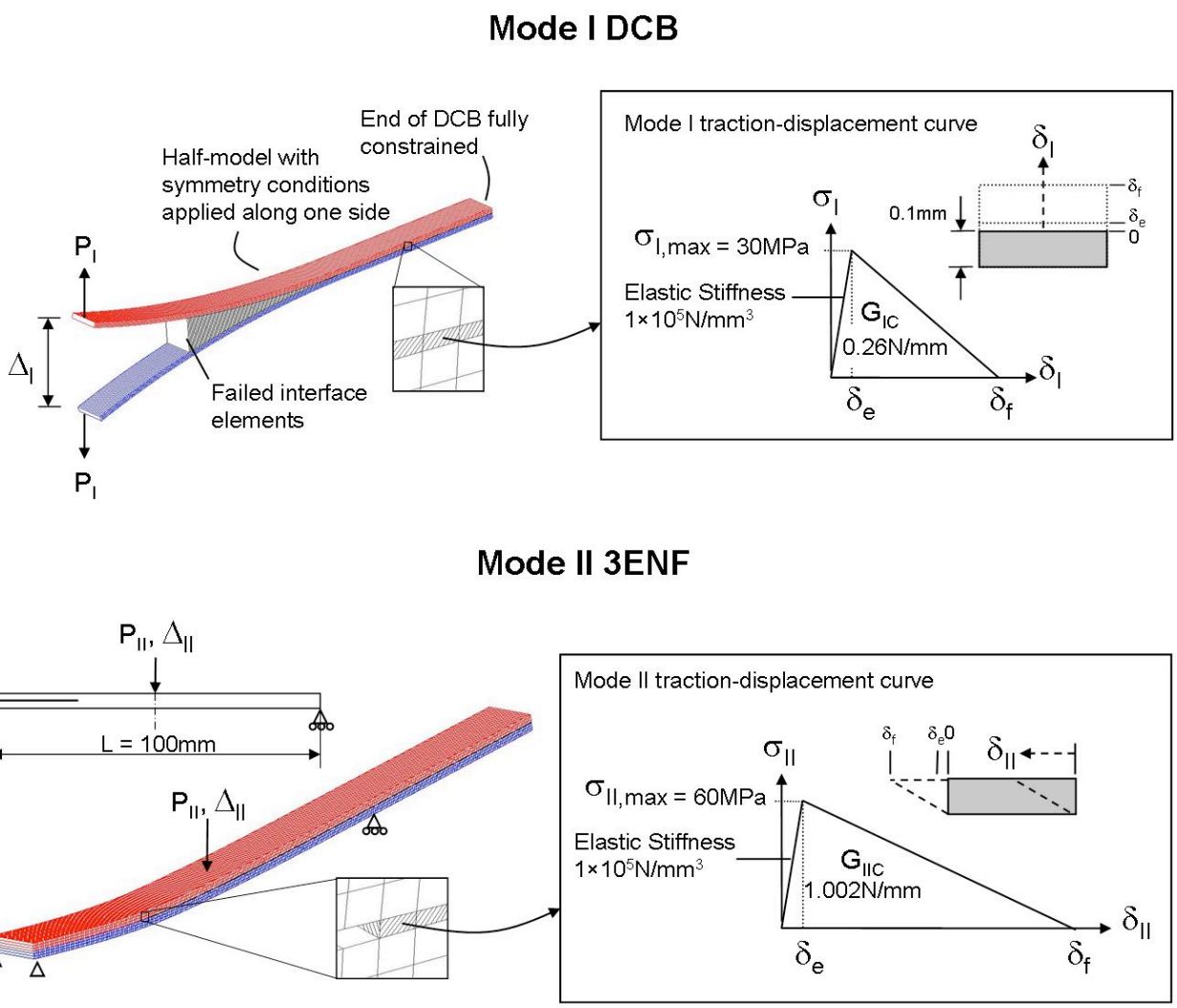

Figure 5: Fracture Toughness Specimen Models and applied loading/boundary conditions

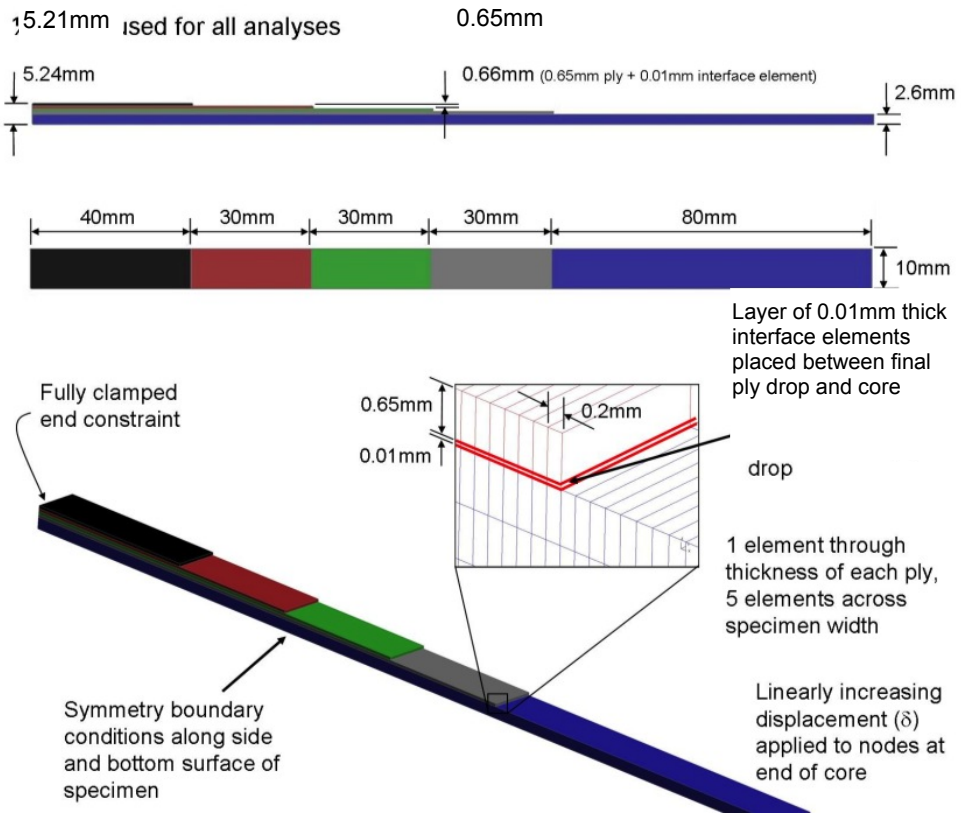

Figure 6: Ply drop model used for interface element analyses

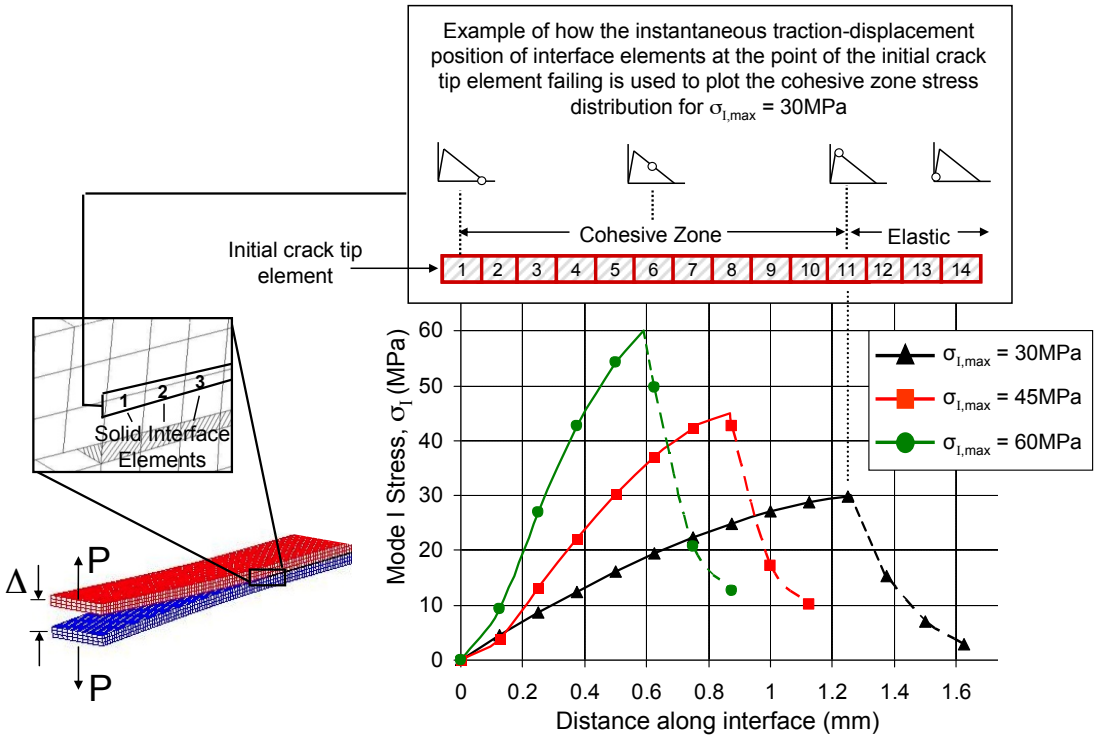

Figure 7: Effect of maximum interfacial stress on cohesive zone length and stress distribution at the point of the initial crack tip element failing for the mode I DCB specimen

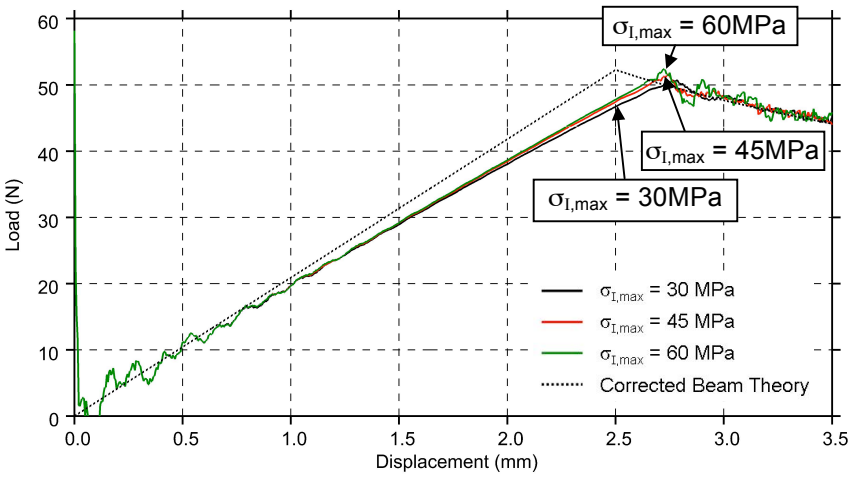

Figure 8: Load-Displacement Analyses for the DCB specimen

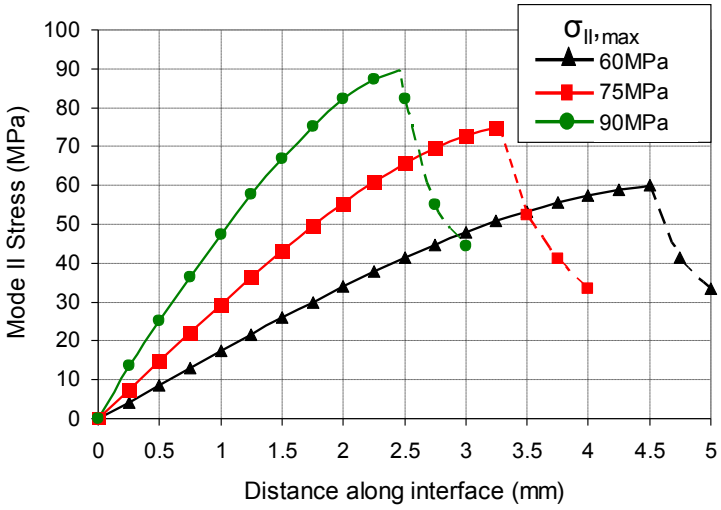

Figure 9: Effect of maximum interfacial stress on cohesive zone length and stress distribution at the point of the initial crack tip element failing for the mode II 3ENF specimen

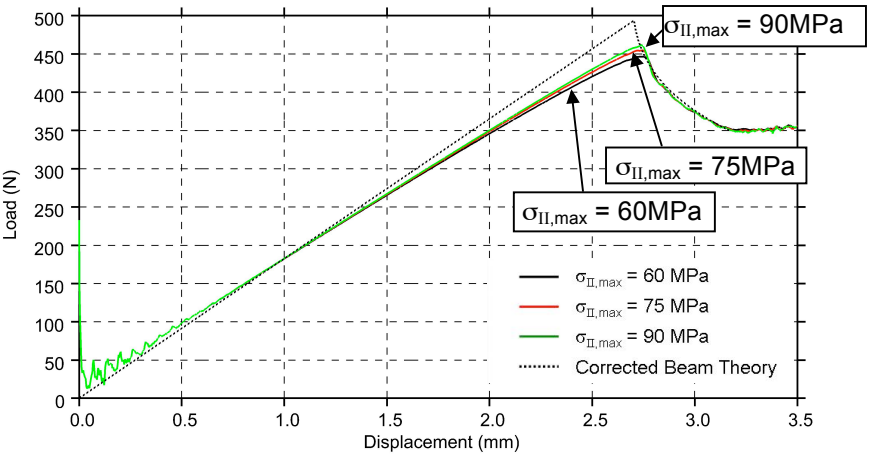

Figure 10: Load-Displacement Analyses for the mode II 3ENF

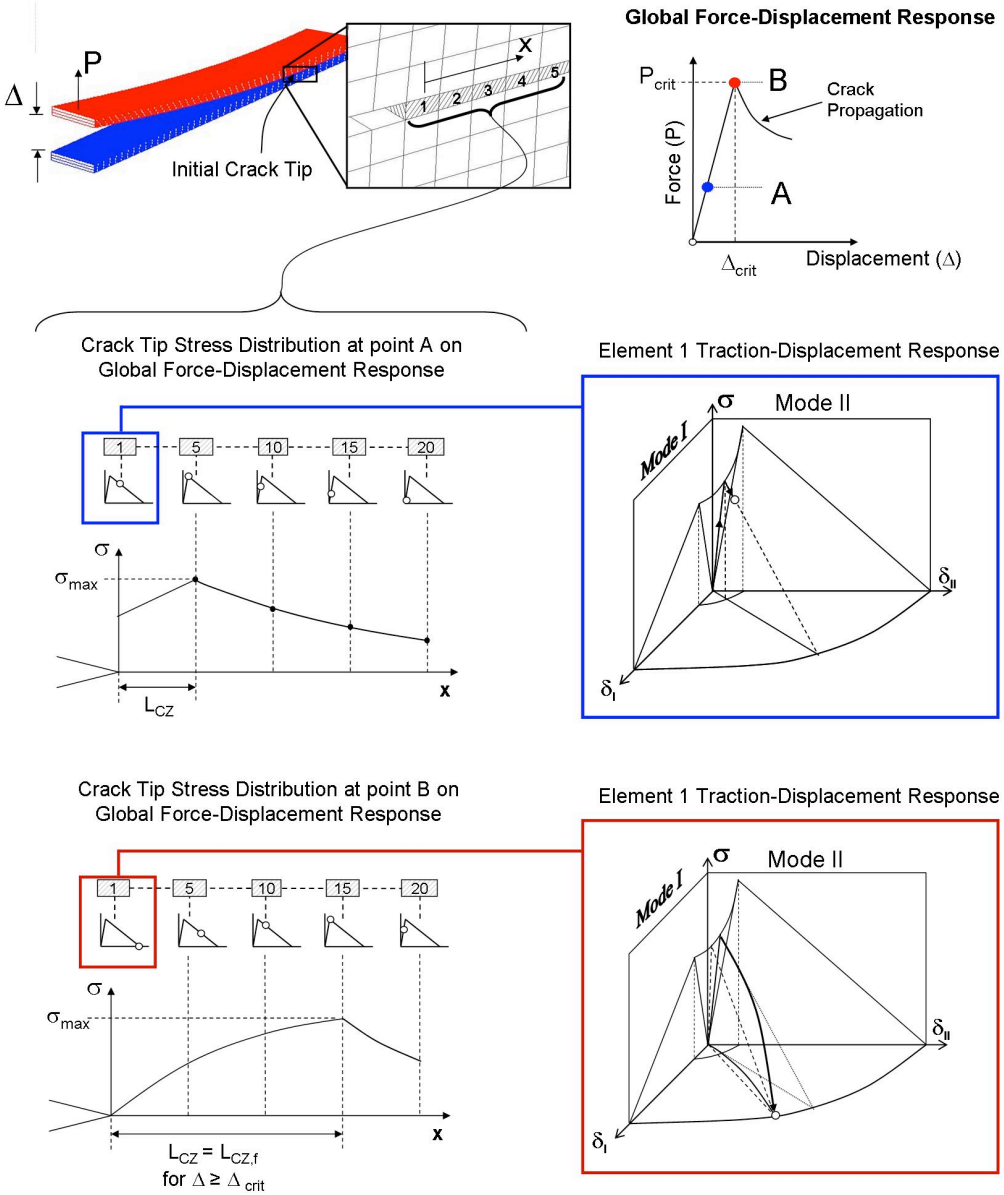

Figure 11: Cohesive zone development in the FRMM specimen

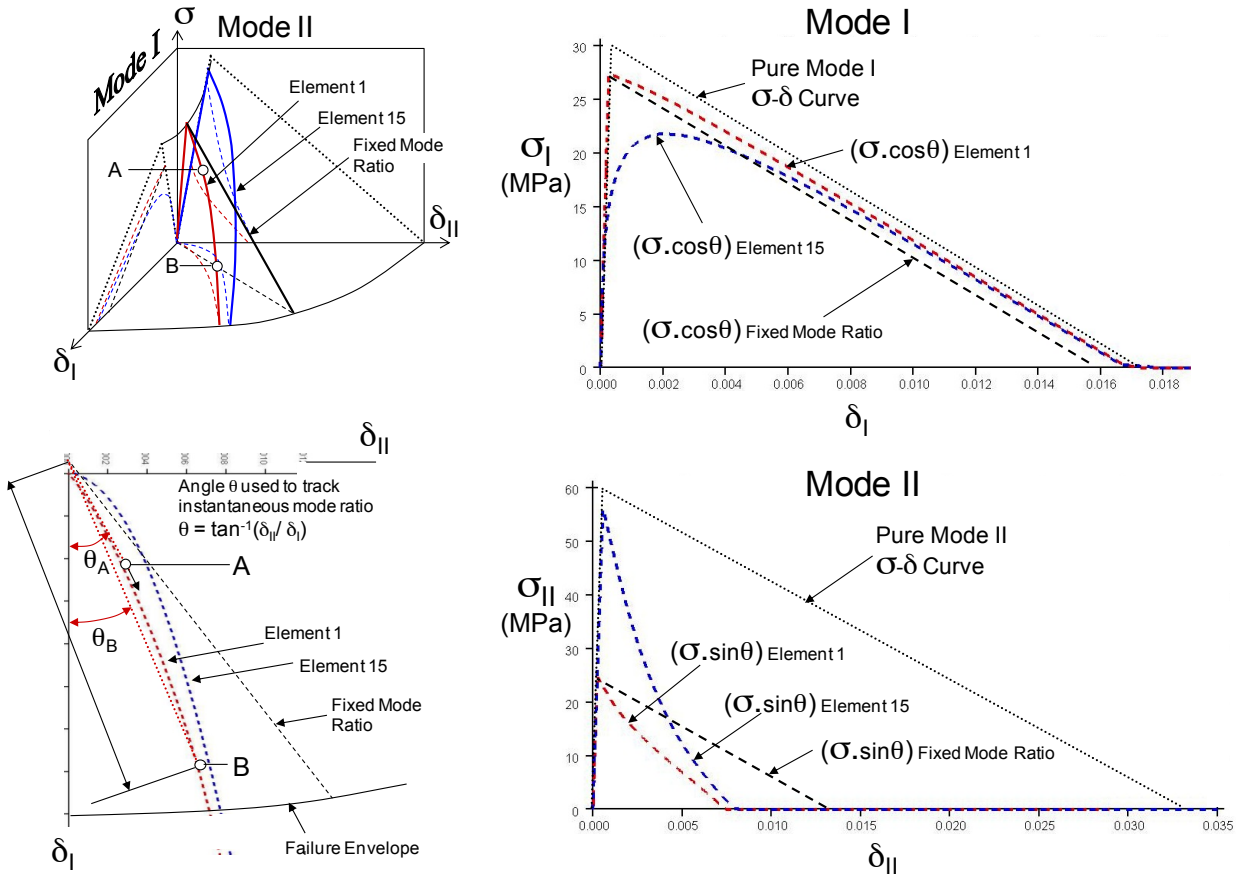

Figure 12: Traction-displacement response of elements 1 (initial crack tip element) and 15 (first element to enter fully developed cohesive zone) for the FRMM specimen

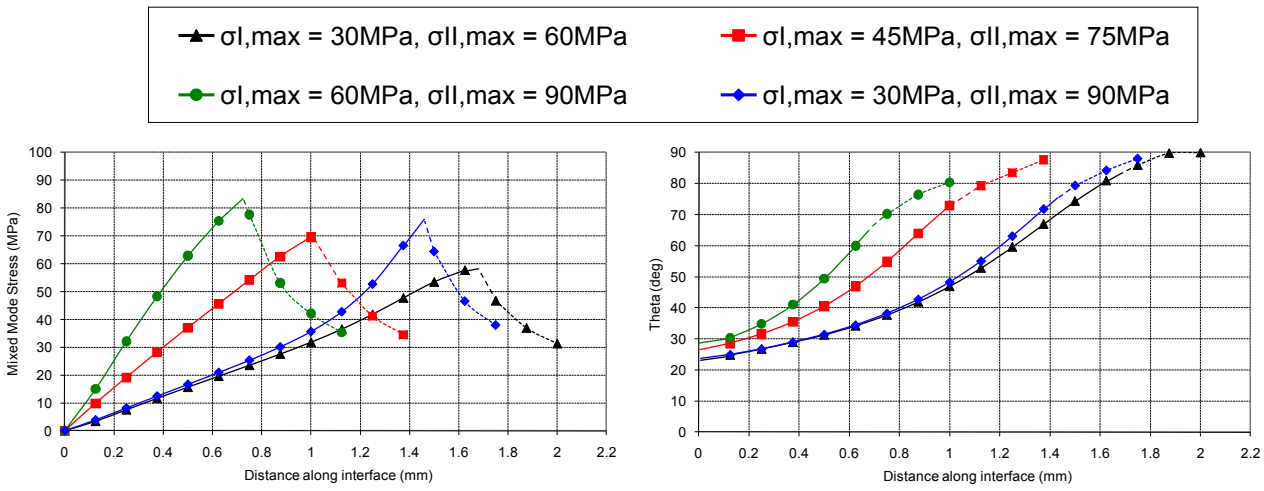

(a) Stress Distribution along Cohesive Zone

(b) Mode-Ratio variation along Cohesive Zone

Figure 13: Effect of maximum interfacial stress on stress distribution and mode ratio across the Cohesive Zone at the point of the initial crack tip element failing for the FRMM specimen

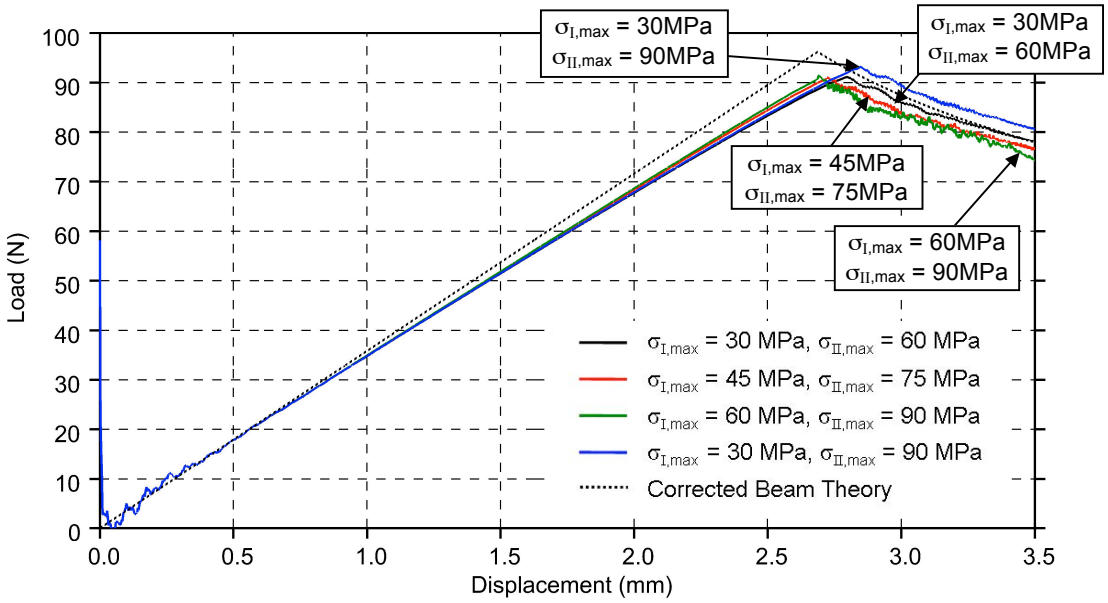

Figure 14: Load-displacement analyses for the FRMM specimen

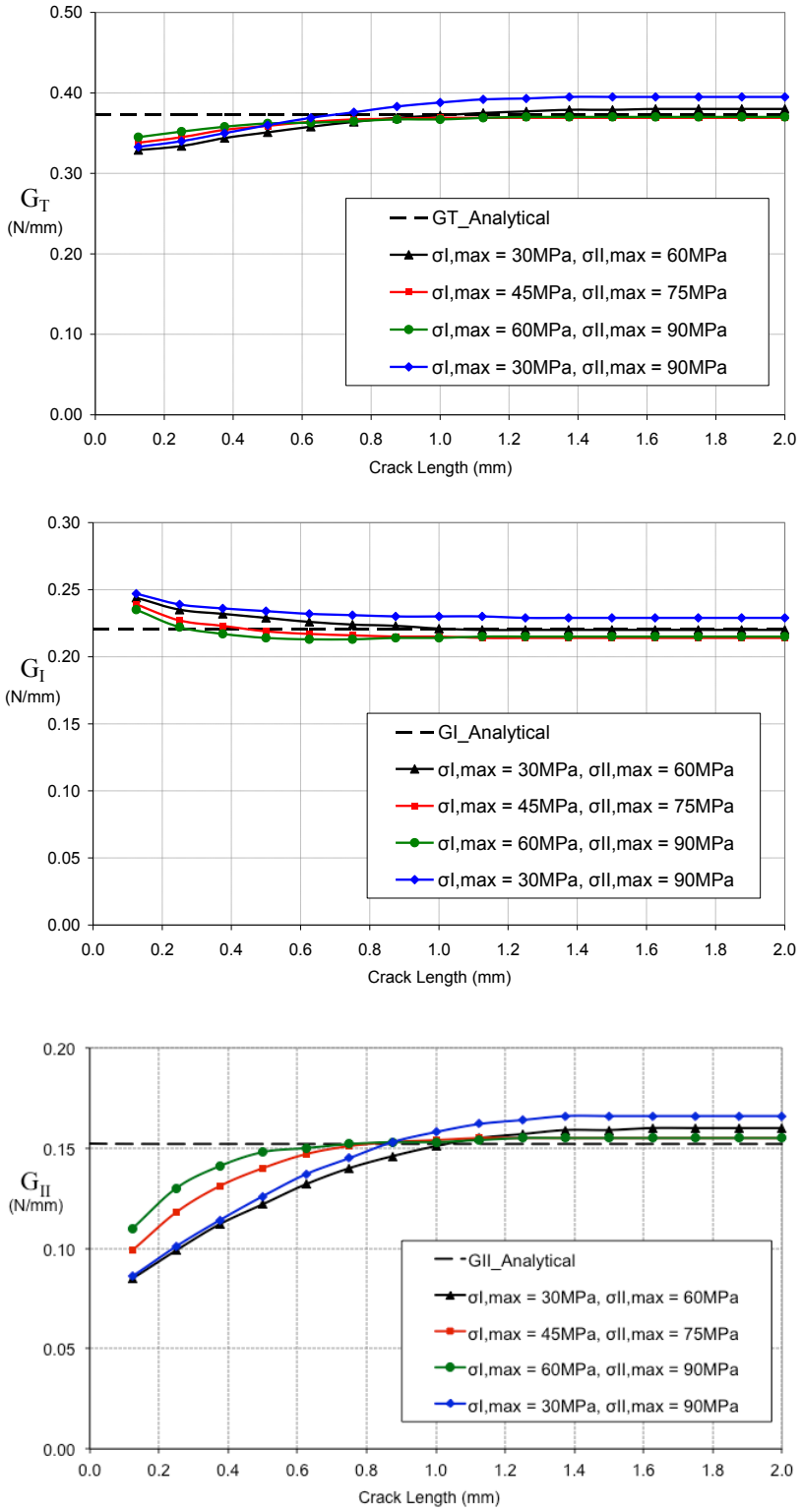

Figure 15: Total energy absorbed by interface elements as crack advances in the FRMM specimen

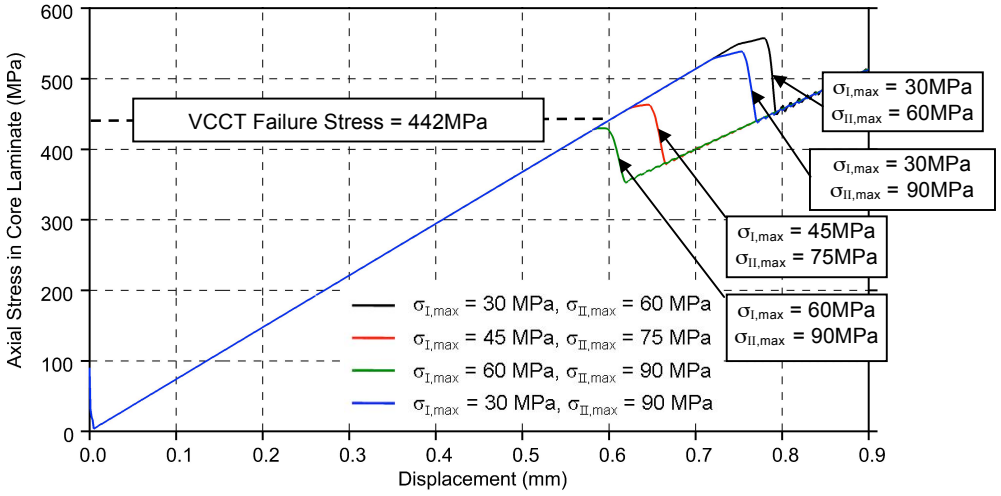

Figure 16: Load-Displacement analyses for external ply drop model using interface elements

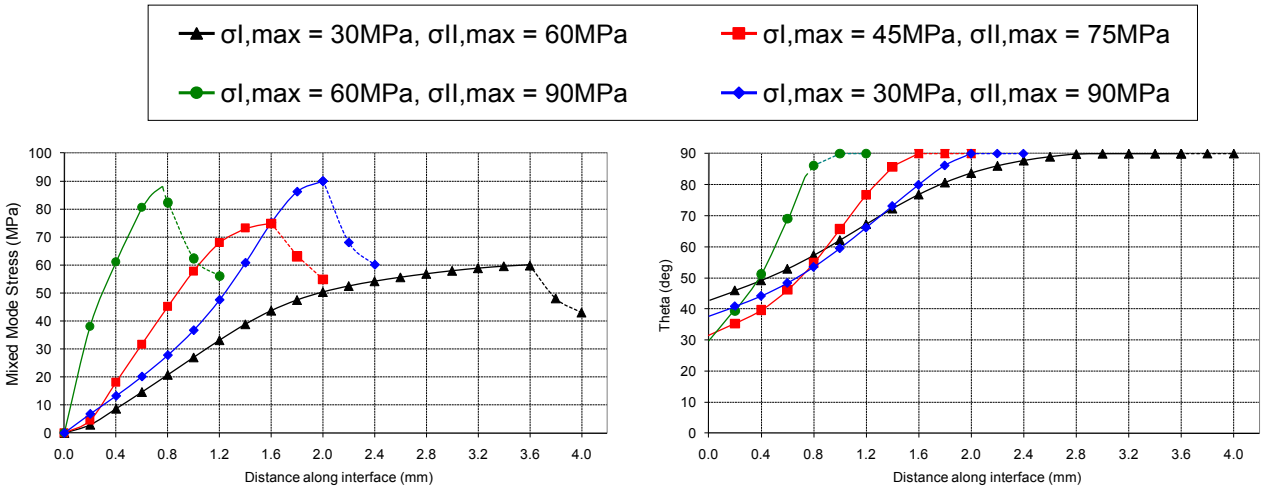

(a) Cohesive Zone Stress Distribution

(b) Mode Ratio Variation

Figure 17: Effect of maximum interfacial stress on stress distribution and mode ratio across the Cohesive Zone at the point of the initial crack tip element failing for the external ply drop specimen

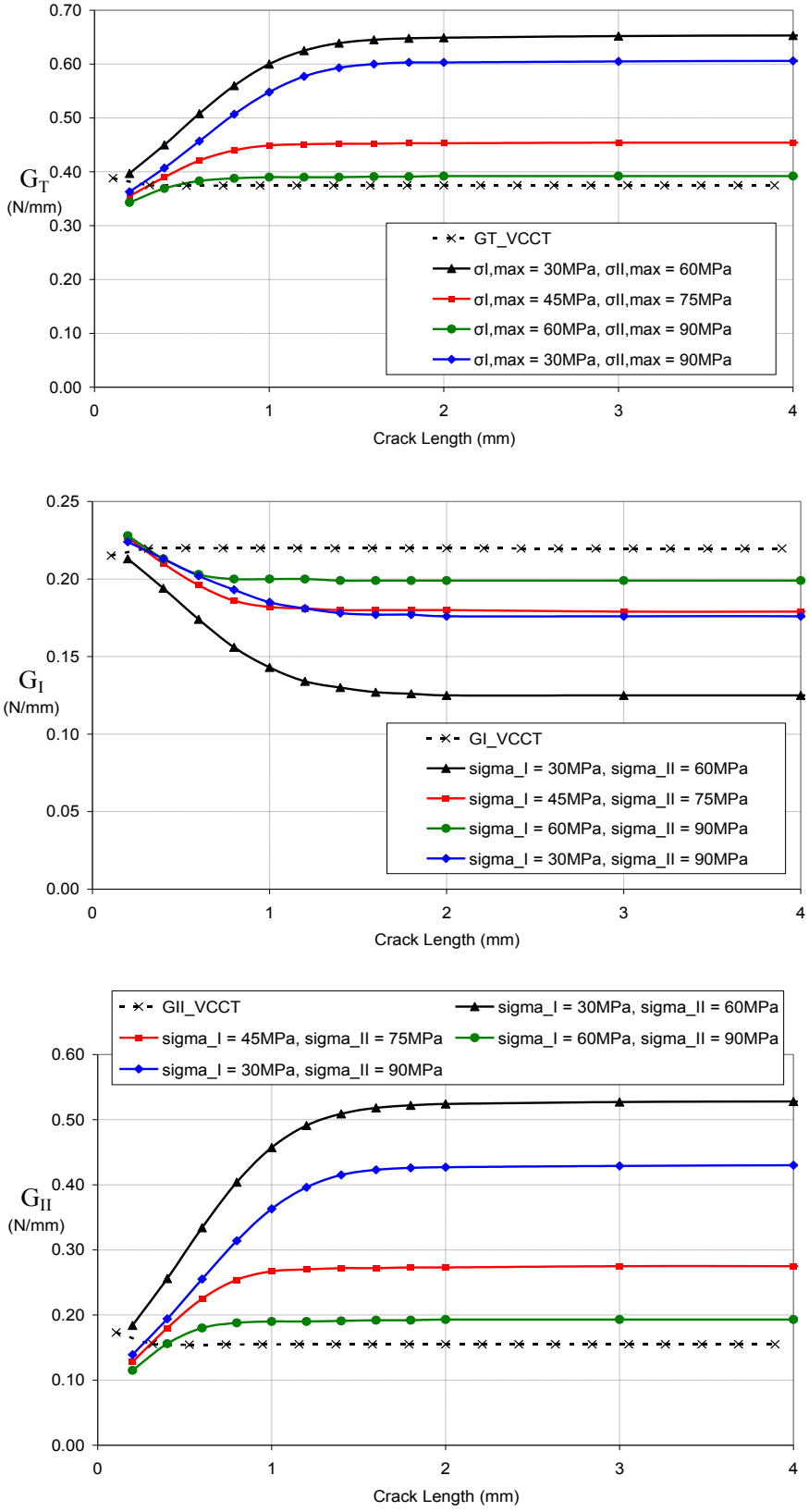

Figure 18: Energy absorbed by interface elements as crack advances in the external ply drop specimen